Chemical Research in Toxicology

Article

pubs.acs.org/crt

Structures of Exocyclic *R,R*- and *S,S*-N^6,N^6-(2,3-Dihydroxybutan-1,4-diyl)-2′-Deoxyadenosine Adducts Induced by 1,2,3,4-Diepoxybutane

Ewa A. Kowal,[†] Uthpala Seneviratne,[‡] Susith Wickramaratne,[‡] Kathleen E. Doherty,[†] Xiangkun Cao,[†] Natalia Tretyakova,[‡] and Michael P. Stone*[,†]

[†]Department of Chemistry, Center in Molecular Toxicology, and Center for Structural Biology, Stevenson Science Center, Vanderbilt University, 2201 West End Avenue, Nashville, Tennessee 37235, United States

[‡]Department of Medicinal Chemistry and Masonic Cancer Center and Department of Chemistry, University of Minnesota, Minneapolis, Minnesota 55455, United States

Supporting Information

ABSTRACT: 1,3-Butadiene (BD) is an industrial and environmental chemical present in urban air and cigarette smoke, and is classified as a human carcinogen. It is oxidized by cytochrome P450 to form 1,2,3,4-diepoxybutane (DEB); DEB bis-alkylates the N^6 position of adenine in DNA. Two enantiomers of bis-N^6-dA adducts of DEB have been identified: *R,R*-N^6,N^6-(2,3-dihydroxybutan-1,4-diyl)-2′-deoxyadenosine (*R,R*-DHB-dA), and *S,S*-N^6,N^6-(2,3-dihydroxybutan-1,4-diyl)-2′-deoxyadenosine (*S,S*-DHB-dA) [Seneviratne, U., Antsypovich, S., Dorr, D. Q., Dissanayake, T., Kotapati, S., and Tretyakova, N. (2010) *Chem. Res. Toxicol. 23*, 1556−1567]. Herein, the *R,R*-DHB-dA and *S,S*-DHB-dA adducts have been incorporated into the 5′-d(C[1]G[2]G[3]A[4]C[5]X[6]A[7]G[8]A[9]A[10]G[11])-3′:5′-d(C[12]T[13]T[14]C[15]T[16]T[17]G[18]T[19]C[20]C[21]G[22])-3′ duplex [X[6] = *R,R*-DHB-dA (R[6]) or *S,S*-DHB-dA (S[6])]. The structures of the duplexes were determined by molecular dynamics calculations, which were restrained by experimental distances obtained from NMR data. Both the *R,R*- and *S,S*-DHB-dA adducts are positioned in the major groove of DNA. In both instances, the bulky 3,4-dihydroxypyrrolidine rings are accommodated by an out-of-plane rotation about the C6-N^6 bond of the bis-alkylated adenine. In both instances, the directionality of the dihydroxypyrrolidine ring is evidenced by the pattern of NOEs between the 3,4-dihydroxypyrrolidine protons and DNA. Also in both instances, the anti conformation of the glycosyl bond is maintained, which combined with the out-of-plane rotation about the C6-N^6 bond, allows the complementary thymine, T[17], to remain stacked within the duplex, and form one hydrogen bond with the modified base, between the imine nitrogen of the modified base and the T[17] N3H imino proton. The loss of the second Watson−Crick hydrogen bonding interaction at the lesion sites correlates with the lower thermal stabilities of the *R,R*- and *S,S*-DHB-dA duplexes, as compared to the corresponding unmodified duplex. The reduced base stacking at the adduct sites may also contribute to the thermal instability.

Major Groove Structures of *R,R*- and *S,S*- N^6,N^6-(2,3-Dihydroxybutan-1,4-diyl)-2′-Deoxyadenosine Adducts in DNA

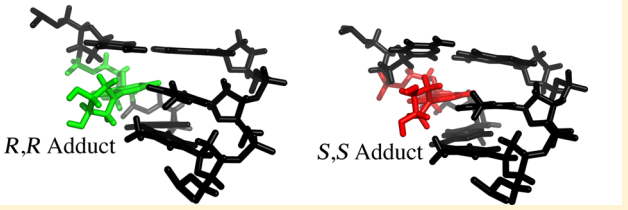

INTRODUCTION

1,3-Butadiene (BD)[1] is used to manufacture styrene-butadiene rubber (SBR).[1,2] Several billion pounds of SBR is produced annually in the United States. It is also a combustion product from automobile emissions[3] and cigarette smoke.[4] BD is genotoxic and is carcinogenic in rodents,[5,6] particularly in mice,[7−9] and less potent in rats.[10−13] These species-specific differences in genotoxicity and carcinogenicity have been attributed to differences in various pathways of BD metabolism.[14] In the SBR industry, occupational exposures to BD are associated with increased risk for hematopoietic cancers.[15−30] Consequently, BD has been classified by the United States Environmental Protection Agency as "carcinogenic to humans by inhalation",[31] and it has been also characterized as a known human carcinogen by the National Toxicology Program.[32] The International Agency for Cancer Research (IARC) lists BD as "carcinogenic to humans (Group 1)."[33,34] Accordingly, there has been interest in identifying biomarkers of exposures to BD.[35,36]

Delineating the molecular basis for BD-induced genotoxicity is complicated by the formation of multiple electrophilic species derived from BD metabolism, their abilities to alkylate multiple sites in DNA, and the stereochemistry of the resulting adducts.[30,37−39] BD is oxidized by cytochrome P450s to form 1,2-epoxy-3-butenes (EB).[40] As shown in Scheme 1, EB can either undergo hydrolysis to form 1,2-dihydroxy-3-butene or further oxidation to 1,2,3,4-diepoxybutane (DEB). Hydrolysis of DEB can form 1,2-dihydroxy-3,4-epoxybutane (EBD). Albertini, Kirman, and co-workers have reviewed BD metabolism and genotoxicity.[30,41,42] Although DEB is a minor metabolite of BD, it is 50- to 100-fold more genotoxic and mutagenic in human cells than the monoepoxide metabolites,

Received: December 19, 2013
Published: April 17, 2014

   dx.doi.org/10.1021/tx400472p | *Chem. Res. Toxicol.* 2014, 27, 805−817

Scheme 1. Cytochrome P450-Mediated Oxidation of BD to Stereoisomeric EB, DEB, and EBD Electrophiles

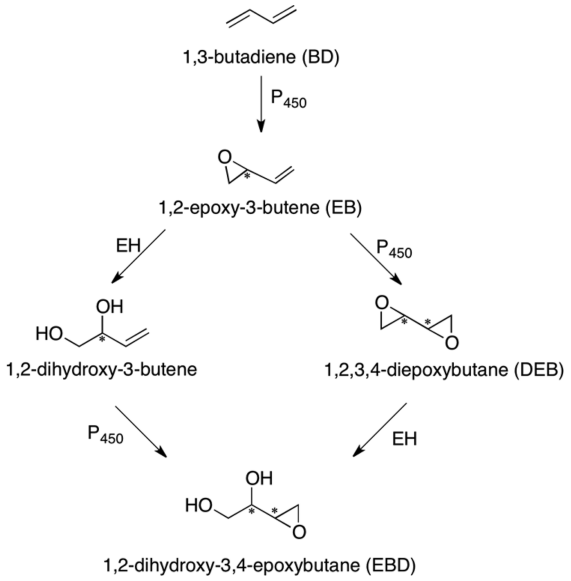

EB and EBD.[43,44] Three stereoisomers of DEB, *S,S*, *R,R*, and *meso*, are generated metabolically.[45] Of these, the *S,S* isomer is the most cytotoxic[46,47] and mutagenic.[48] In mice, levels of DEB have been measured at ~250 pmol/g in blood.[49] While the genotoxicity of DEB has been attributed to its ability to cross-link DNA via the N7 position of guanine,[50,51] it induces a significant number of A to T transversions,[44,52,53] suggesting the formation of adenine adducts. A number of these have been identified, including the stereospecific *R,R*- and *S,S*-N^6,N^6-(2,3-dihydroxybutan-1,4-diyl)-2′-deoxyadenosine adducts (N^6,N^6-DHB-dA),[54] which arise from bis-alkylation of the N^6 exocyclic amino groups of adenines in DNA by *R,R*- and *S,S* -DEB (Chart 1).

Presently, we have used NMR spectroscopy to determine the structures of the *R,R*- and *S,S*-N^6,N^6-DHB-dA adducts[54] incorporated into the oligodeoxynucleotide duplexes 5′-d($C^1G^2G^3A^4\underline{C}^{\underline{S}}\underline{R}^{\underline{6}}\underline{A}^{\underline{Z}}G^8A^9A^{10}G^{11}$)-3′:5′-d($C^{12}T^{13}T^{14}C^{15}T^{16}T^{17}$-$G^{18}T^{19}C^{20}C^{21}G^{22}$)-3′ (R = *R,R*-DHB-dA) and 5′-d($C^1G^2G^3$-$A^4\underline{C}^{\underline{S}}\underline{S}^{\underline{6}}\underline{A}^{\underline{Z}}G^8A^9A^{10}G^{11}$)-3′:5′-d($C^{12}T^{13}T^{14}C^{15}T^{16}T^{17}G^{18}$-$T^{19}C^{20}C^{21}G^{22}$)-3′ (S = *S,S*-DHB-dA) (Chart 1). The sequence of these duplexes arises from codon 61 and the surrounding sequence of the *ras* proto-oncogene, and the unmodified duplex has been spectroscopically characterized and examined as to its structure in solution.[55] As compared to the unmodified duplex, both the *R,R*-DHB-dA and *S,S*-DHB-dA adducts thermally destabilize the DNA. The structures of the duplexes containing either the R^6 or S^6 adducts shows that, in both instances, the DHB moiety rotates around the C6-N^6 bond and is located in the major groove of DNA. DHB-dA adducts can only form one Watson−Crick hydrogen bond, between N1 of R^6 or S^6 and the T^{17} N3H imino proton in the complementary strand. These results reveal that the R^6 and S^6 DHB-dA adducts destabilize DNA by disrupting Watson−Crick hydrogen bonding and affecting stacking interactions with neighboring base pairs.

MATERIALS AND METHODS

Synthesis of Modified Oligodeoxynucleotides. The 2′-deoxyribonucleoside-3′-phosphoramidites iPr-PAC-dG-CE, PAC-dA-CE, and Ac-dC-CE, dT-CE, the iPr-PAC-dG-CPG ABI columns, and other reagents necessary for automated DNA synthesis were purchased from Glen Research (Sterling, VA). The 5′-*O*-(4,4′-dimethoxytrityl)-3′-*O*-(2-cyanoethyl)-*N,N*-diisopropyl phosphoramidite of the 6-chloropurine-2′-deoxyriboside was purchased from ChemGenes Co. (Wilmington, MA). Oligodeoxynucleotides were synthesized by solid phase methods using an ABI 394 DNA synthesizer (Life Technologies, Carlsbad, CA). All solvents and chemical reagents were obtained from commercial sources and used without further purification. The modified oligodeoxynucleotides 5′-d(CGGAC<u>R</u>AGAAG)-3′ and 5′-d(CGGAC<u>S</u>AGAAG)-3′ containing site- and stereospecific N^6,N^6-DHB-dA lesions were synthesized by a postoligomerization approach,[56] which was originally developed by Harris, and co-workers.[57−59] Briefly, 11-mer oligodeoxynucleotides containing a site-specific 6-chloropurine at position R^6 or S^6 (100 nmol) were coupled with (*R,R*)- or (*S,S*)-pyrrolidine-3,4-diol (20 mg), respectively, in the presence of DIPEA (200 μL) in DMSO (300 μL) for 72 h at 37 °C. The resulting structurally modified oligodeoxynucleotides were purified and desalted by reverse phase HPLC, characterized by capillary HPLC-ESI-MS, and quantified by UV spectrophotometry. Sequence and site-specificity were confirmed by MALDI-MS of partial exonuclease digests.[56]

The unmodified oligodeoxynucleotides 5′-d(CGGACAAGAAG)-3′ and 5′-d(CTTCTTGTCCG)-3′ were synthesized by the Midland Reagent Company (Midland, TX) and purified by anion-exchange HPLC. The oligodeoxynucleotides were purified using a semi-preparative scale reverse-phase HPLC column (YMC, Kyoto, Japan, Phenyl-Hexyl, 5 μm, 250 mm ×10.0 mm) equilibrated with 0.1 M ammonium formate (pH 7.0) using an acetonitrile gradient. The oligodeoxynucleotides were desalted by elution from Sephadex G-25, lyophilized, and characterized by MALDI-TOF-MS.

The concentrations of single-stranded oligodeoxynucleotides were determined by UV absorbance at 260 nm using extinction coefficients of 118,300 L $M^{-1}cm^{-1}$ for strands 5′-d(CGGAC<u>R</u>AGAAG)-3′, 5′-d(CGGAC<u>S</u>AGAAG)-3′, and 5′-d(CGGACAAGAAG)-3′ and assum-

Chart 1. (A) Structures of the *R,R*-DHB-dA and *S,S*-DHB-dA Adducts, and (B) Sequences and Numbering of the Unmodified and Modified Duplexes[a]

A

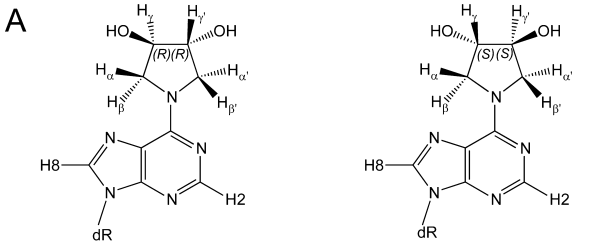

R,R-DHB-dA
(*R,R*)-N^6,N^6-(2,3-dihydroxybutan-1,4-diyl)-2′-deoxyadenosine

S,S-DHB-dA
(*S,S*)-N^6,N^6-(2,3-dihydroxybutan-1,4-diyl)-2′-deoxyadenosine

B

Unmodified duplex

5′-d(C^1 G^2 G^3 A^4 C^5 A^6 A^7 G^8 A^9 $A^{10}G^{11}$)-3′
3′-d($G^{22}C^{21}C^{20}T^{19}G^{18}T^{17}T^{16}C^{15}T^{14}T^{13}C^{12}$)-5′

R,R duplex

5′-d(C^1 G^2 G^3 A^4 C^5 **R^6** A^7 G^8 A^9 $A^{10}G^{11}$)-3′
3′-d($G^{22}C^{21}C^{20}T^{19}G^{18}T^{17}T^{16}C^{15}T^{14}T^{13}C^{12}$)-5′

S,S duplex

5′-d(C^1 G^2 G^3 A^4 C^5 **S^6** A^7 G^8 A^9 $A^{10}G^{11}$)-3′
3′-d($G^{22}C^{21}C^{20}T^{19}G^{18}T^{17}T^{16}C^{15}T^{14}T^{13}C^{12}$)-5′

[a]In A, H_α and $H_{\alpha'}$ are pro-R protons; and H_β, $H_{\beta'}$ are pro-S protons. In B, at the 6th position adenine was replaced with adduct R^6 (*R,R*-DHB-dA) to form the *R,R*-duplex or adduct S^6 (*S,S*-DHB-dA) to form the *S,S*-duplex.

dx.doi.org/10.1021/tx400472p | *Chem. Res. Toxicol.* 2014, 27, 805−817

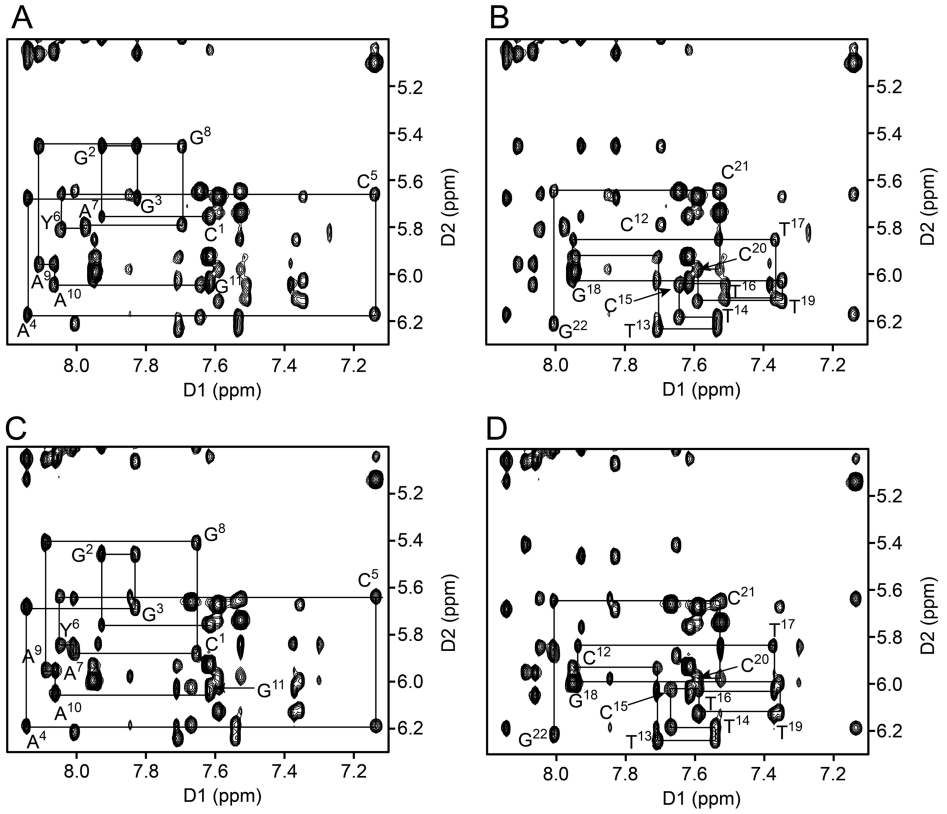

Figure 1. NOESY spectra for the *R,R*- and *S,S*-DHB-dA modified-duplexes, showing sequential NOEs between the base aromatic and anomeric protons. (A) The modified strand for the *R,R*-duplex, showing nucleotides C^{1} to G^{11}. (B) The complementary strand for the *R,R*-duplex, showing nucleotides C^{12} to G^{22}. (C) The modified strand for the *S,S*-duplex, showing nucleotides C^{1} to G^{11}. (D) The complementary strand for the *S,S*-duplex, showing nucleotides C^{12} to G^{22}. Spectra were obtained at 800 MHz with a mixing time of 250 ms at 15 °C.

ing similar extinction coefficients for N^6,N^6-DHB-dA and dA, and 90,800 L $M^{-1}cm^{-1}$ for the complementary strand 5′-d-(CTTCTTGTCCG)-3′.[60] To assemble the respective duplexes, the complementary strand 5′-d(CTTCTTGTCCG)-3′ was combined with equal molar quantities of either 5′-(CGGACAAGAAG)-3′, 5′-d(CGGACRAGAAG)-3′, or 5′-d(CGGACSAGAAG)-3′, heated to 75 °C for 15 min, and cooled to room temperature to form the unmodified, and *R,R*- and *S,S*-duplexes, respectively.

UV Melting Studies. Absorption vs temperature profiles (UV melts) for each duplex were measured using a Varian Cary 100 Bio spectrophotometer (Varian Associates, Palo Alto, CA). The concentrations of the duplexes were 2.1 μM. Samples were prepared in a buffered solution of 10 mM NaH_2PO_4 (pH 7.0) and 50 μM Na_2EDTA containing either 0.1 M NaCl or 1 M NaCl. The temperature was increased from 5 to 85 °C for each duplex at a rate of 0.50 °C/min. The UV absorbance was monitored at 260 nm.

NMR Spectroscopy. The modified double-stranded duplexes containing the R^6 or S^6 adducts were prepared in 10 mM NaH_2PO_4 (pH 7.0) containing 0.1 M NaCl and 50 μM Na_2EDTA at 0.7 mM and 0.4 mM concentrations, respectively. To observe the nonexchangeable protons, the duplexes were exchanged with D_2O and dissolved in 99.96% D_2O. For the observation of exchangeable protons, the samples were dissolved in 9:1 H_2O:D_2O. ^1H NMR spectra were recorded using 800 MHz, 600 MHz, and 500 MHz spectrometers equipped with cryogenic probes (Bruker Biospin Inc., Billerica, MA). Chemical shifts were referenced to the chemical shift of water resonance at the corresponding temperature, with respect to 4,4-dimethyl-4-silapentane-1-sulfonic acid (DSS). Data were processed using the program TOPSPIN (Bruker Biospin Inc., Billerica, MA). The NOESY[61,62] and DQF-COSY[63] spectra in D_2O were collected at 15 °C at 800 MHz and for the unmodified duplex only at 600 MHz; NOESY experiments were conducted at a mixing time of 60, 150, 200, and 250 ms. These experiments were performed with a relaxation delay of 2.0 s. The NOESY spectra in 9:1 H_2O:D_2O were collected at 5 °C at 500 MHz for modified duplexes and 600 MHz for the unmodified duplex, with a 250 ms mixing time. NMR experiments in 9:1 H_2O:D_2O were collected at 5, 10, 15, 20, 25, and 30 °C at 800 MHz for the *S,S*-duplex, and 600 MHz for the *R,R* and unmodified duplexes. These experiments were performed with a relaxation delay of 1.5 s. Water suppression was performed using the WATERGATE pulse sequence.[64]

NMR Experimental Restraints. The NOESY spectra of the duplexes measured in D_2O were processed using the TOPSPIN software and were evaluated using the program SPARKY[65] to obtain the cross-peak assignments. The cross-peak intensities were measured by volume integrations. The peak volumes were divided into classes based on the confidence in integrations of the cross-peaks. For well-resolved strong nonoverlapping cross-peaks, a volume integration error of 10% was assigned. For weaker or more overlapping cross-peaks, for which the confidence in volume integration was lower, errors of 20, 30, 40, or 50% were applied. Experimental intensities were combined with intensities calculated from complete relaxation matrix analysis of a starting model to generate a hybrid intensity matrix.[66,67] Conversion from peak volumes into distances, including upper and lower bounds, was completed using the program MARDIGRAS,[68] which refined the hybrid intensity matrix.[68] For methyl protons, the JUMP 3[69] model was employed. Calculations were performed using 150, 200, and 250 ms mixing time data and 2, 3, and 4 ns isotropic correlation times. Evaluations of these results, e.g., for spin diffusion effects, provided distance restraints used for restrained molecular dynamics (rMD) calculations. Additional empirical restraints were obtained from canonical values derived from B-DNA.[70] Empirical Watson−Crick base pair restraints were employed with the exception of the modified base pairs. Pseudorotation restraints were also used, but with the exceptions of the terminal bases C^1, G^{11}, C^{12}, G^{22}, and the modified nucleotides R^6 or S^6.

dx.doi.org/10.1021/tx400472p | *Chem. Res. Toxicol.* 2014, 27, 805−817

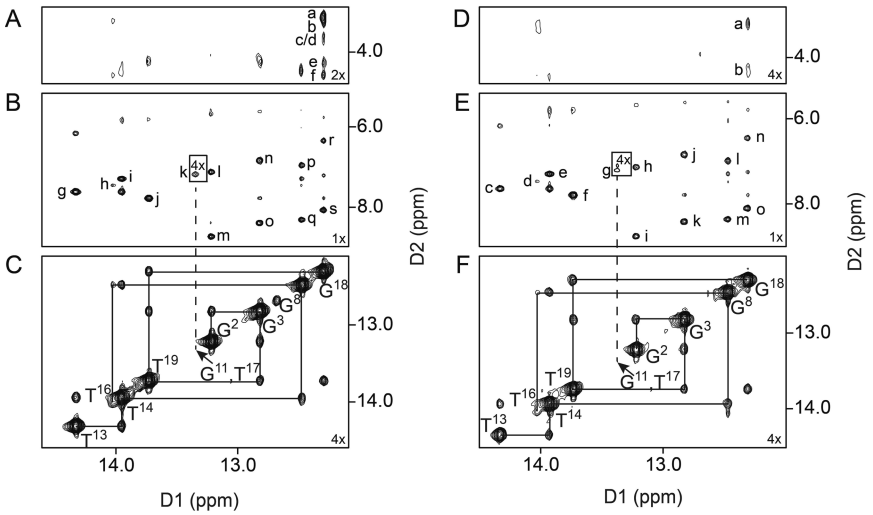

Figure 2. NOESY spectra for the *R,R*- and *S,S*-duplexes, showing NOEs between the base imino protons and the amino protons, and DHB protons. (A) Interstrand NOEs between the R^6 adduct and the G^{18} base. The cross-peaks are assigned as a, R^6 $H_{\beta'/\alpha'}$ → G^{18} N1H; b, R^6 $H_{\beta'/\alpha'}$ → G^{18} N1H; c, R^6 $H_{\beta/\alpha}$ → G^{18} N1H; d, R^6 $H_{\beta/\alpha}$ → G^{18} N1H; e, R^6 $H_{\gamma'}$ → G^{18} N1H; and f, R^6 H_{γ} → G^{18} N1H. (B) Interstrand NOEs between complementary bases. The cross-peaks are assigned as g, A^{10} H2 → T^{13} N3H; h, A^7 H2 → T^{16} N3H; i, A^9 H2 → T^{14} N3H; j, A^4 H2 → T^{19} N3H; k, R^6 H2 → T^{17} N3H and C^{12} N^2 H1 → G^{11} N1H; l, C^{21} N^2H1 → G^2 N1H; m, C^{21} N^2H2 → G^2 N1H; n, C^{20} N^2H1 → G^3 N1H; o, C^{20} N^2H2 → G^3 N1H; p, C^{15} N^2H1 → G^8 N1H; q, C^{15} N^2H2 → G^8 N1H; r, C^5 N^2H1 → G^{18} N1H; and s, C^5 N^2H2 → G^{18} N1H. The intensity of the cross-peak k in the black box is lower than the rest of the cross-peaks, and the contour of this section was adjusted to be visible in the plot. (C) NOE connectivity for the imino protons for the base pairs G^2:C^{21}, G^3:C^{20}, A^4:T^{19}, C^5:G^{18}, A^7:T^{16}, G^8:C^{15}, A^9:T^{14}, and A^{10}:T^{13}. The cross-peaks are T^{13} N3H → T^{14} N3H, T^{14} N3H → G^8 N1H, G^8 N1H → T^{16} N3H, G^{18} N1H → T^{19} N3H, T^{19} N3H → G^3 N1H, and G^3 N1H → G^2 N1H. For clarity, in panel A the contours are represented at 2× the intensity of those in panel B, in panel B the contour of cross-peak k (in black box) is presented at 4× the intensity of the remainder of the cross-peaks, and in panel C the contours are represented at 4× the intensity of those in panel B. (D) Interstrand NOEs between the S^6 nucleotide and G^{18}. The cross-peaks are assigned as a, S^6 $H_{\alpha',\beta'}$, $H_{\alpha,\beta}$ → G^{18} N1H; and b, S^6 $H_{\alpha,\beta}$, $H_{\gamma'}$ → G^{18} N1H. (E) Interstrand NOEs between complementary bases. The cross-peaks are assigned as c, A^{10} H2 → T^{13} N3H; d, A^7 H2 → T^{16} N3H; e, A^9 H2 → T^{14} N3H; f, A^4 H2 → T^{19} N3H; g, S^6 H2 → T^{17} N3H and C^{12} N^2 H1 → G^{11} N1H; h, C^{21} N^2H1 → G^2 N1H; i, C^{21} N^2H2 → G^2 N1H; j, C^{20} N^2H1 → G^3 N1H; k, C^{20} N^2H2 → G^3 N1H; l, C^{15} N^2H1 → G^8 N1H; m, C^{15} N^2H2 → G^8 N1H; n, C^5 N^2H1 → G^{18} N1H; and o, C^5 N^2H2 → G^{18} N1H. (F) NOE connectivity for the imino protons for the base pairs G^2:C^{21}, G^3:C^{20}, A^4:T^{19}, C^5:G^{18}, A^7:T^{16}, G^8:C^{15}, A^9:T^{14}, and A^{10}:T^{13}. The cross-peaks are T^{13} N3H → T^{14} N3H, T^{14} N3H → G^8 N1H, G^8 N1H → T^{16} N3H, G^{18} N1H → T^{19} N3H, T^{19} N3H → G^3 N1H, and G^3 N1H → G^2 N1H. For clarity, in panel D the contours are represented at 4× the intensity of those in panel E, in panel E the contour of cross-peak g (black box) is presented at 4× the intensity of the remainder of the cross-peaks, and in panel F the contours are represented at 4× the intensity of those in panel E. The spectra were obtained at 500 MHz with a mixing time of 250 ms at 5 °C.

For unmodified nucleotides, empirical phosphodiester backbone angles were restrained by square well potentials with widths of ±60°. For the modified nucleotides R^6 or S^6, the widths of the square well potentials were increased to ±120°.

Restrained Molecular Dynamics Calculations. A B-type DNA duplex was constructed. The adenine at position A^6 was replaced by either the R^6 or the S^6 adduct using the program INSIGHT II (Accelrys Inc., San Diego, CA). The program AMBER,[71] including the parm99 force field,[72] was used. Partial charges for the *R,R*- and *S,S*-DHB-dA adducts were calculated with the B3LYP/6-31G* basis set in GAUSSIAN,[73] and they were employed in the parameter files prepared in the program XLEAP.[74] Tables S1 and S2 in the Supporting Information provide the parametrization utilized for the *R,R*- and *S,S*-DHB-dA nucleotides. The modified duplexes were each subjected to 1000 cycles of potential energy minimization. The simulated annealing protocol[75] used for the rMD calculations utilized force constants of 32 kcal mol^{-1} $Å^{-2}$ for distance restraints. The generalized Born model[76] was used for solvation. The salt concentration was 0.1 M. The molecule was coupled to the bath temperature to establish the temperature during simulated annealing calculations.[77] Initially, calculations were performed for 20 ps (20,000 steps). For the first 1,000 steps, the system was heated from 0 to 600 K with a coupling of 0.5 ps, followed by 1,000 steps at 600 K, followed by 16,000 steps in which the system was cooled to 100 K with a coupling of 4 ps. In the last 2,000 steps, additional cooling was applied from 100 to 0 K with a coupling of 1 ps. Subsequently, a 100,000 step calculation was performed over 100 ps. For the first 5,000 steps, the system was heated from 0 to 600 K with a coupling of 0.5 ps, followed by 5,000 steps at 600 K, followed by 80,000 during which the system was cooled to 100 K with a coupling of 4 ps, followed by additional cooling for the last 10,000 steps with a coupling of 1 ps. Structure coordinates were saved after each cycle. Complete relaxation matrix analysis (CORMA)[66,67] was used to compare NOE intensities calculated from these emergent structures with the experimentally measured distances. For each modified duplex, eight structures were chosen, based on the lowest deviations from the experimental distance and dihedral restraints. These were subjected to potential energy minimization, and used to obtain average refined structures. Helicoidal analyses were performed using the CURVES+ web server.[78]

Data Deposition. The structure factors and coordinates were deposited in the Protein Data Bank (www.rcsb.org). The PDB ID code for the duplex containing the *R,R*-DHB-dA adduct is 2MHX, and for the duplex containing the *S,S*-DHB-dA adduct the PDB ID code is 2MHZ.

RESULTS

UV Melting Studies. The unfolding of the duplexes was studied by temperature-dependent UV spectroscopy, monitored at 260 nm. The T_m values were determined by taking the first derivatives of the melting curves and shape analyses. For the unmodified duplex, at a concentration of 2.1 μM in 0.1 M NaCl at pH 7, the T_m was 44 °C. At the same concentration and under the same conditions, the T_m for the *R,R*-duplex was 28 °C and for the *S,S*-duplex was 27 °C. Thus, both the *R,R*- and *S,S*-duplexes resulted in similar thermal destabilization of

dx.doi.org/10.1021/tx400472p | Chem. Res. Toxicol. 2014, 27, 805−817

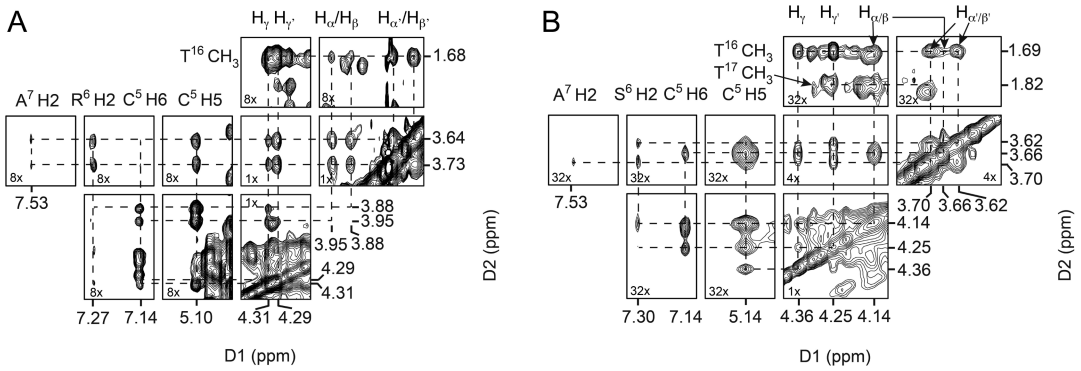

Figure 3. Expanded plot of the NOESY spectrum of the *R,R*- and *S,S*-DHB-dA modified-duplexes, showing assignments of the adduct protons and cross-peaks from the adduct protons to neighbor base protons. (A) The *R,R*-DHB-dA-duplex. The chemical shifts for each proton are A^7 H2, 7.53 ppm; R^6 H2, 7.27 ppm; C^5 H6, 7.14 ppm; C^5 H5, 5.10 ppm; R^6 H_{γ}, 4.31 ppm; and R^6 $H_{\gamma'}$, 4.29 ppm; R^6 H_{α} and R^6 H_{β} could not be unequivocally assigned. They are observed at 3.95 and 3.88 ppm. R^6 $H_{\alpha'}$ and R^6 $H_{\beta'}$ could not be unequivocally assigned. They are observed at 3.73 and 3.64 ppm. T^{16} CH_3, 1.68 ppm. The dashed lines show the NOE connectivity for each proton. For clarity, in the regions with black borders the contours are represented at 8× and 1× the intensity, which is indicated in the corner of each region. (B) The *S,S*-DHB-dA-duplex. The chemical shifts for each proton are A^7 H2, 7.53 ppm; S^6 H2, 7.30 ppm; C^5 H6, 7.14 ppm; C^5 H5, 5.14 ppm; S^6 H_{γ}, 4.36 ppm; and S^6 $H_{\gamma'}$, 4.25 ppm; S^6 H_{α} and S^6 H_{β} could not be unequivocally assigned and were observed at 3.66 and 4.14 ppm; S^6 $H_{\alpha'}$ and S^6 $H_{\beta'}$ could not be unequivocally assigned and were observed at 3.62 and 3.70 ppm; T^{17} CH_3, 1.82 ppm; and T^{16} CH_3, 1.69 ppm. The dashed lines show connectivity for each proton. For picture clarity, in the regions the contours are represented at 32× and 4×, and 1× the intensity, which is indicated in the corner of each region. For both samples spectra were obtained at 800 MHz, with a mixing time of 250 ms. The temperature was 15 °C.

the DNA, irrespective of adduct stereochemistry. The T_m experiments were repeated in 1 M NaCl at pH 7. Under these conditions, the T_m of the unmodified duplex was 53 °C, while the melting temperatures of the *R,R*- and *S,S*-duplexes were 36 and 35 °C, respectively. Again, both the *R,R*- and *S,S*-duplexes thermally destabilized the DNA, to approximately the same extent for both-duplexes, irrespective of adduct stereochemistry.

NMR Spectroscopy of the *R,R*-DHB-dA Duplex. *Base Proton Assignments.* Figure 1 (panels A and B) shows the region of the NOESY spectrum including the base aromatic proton resonances and deoxyribose H1′ proton resonances[79,80] for the modified strand C^1 → G^{11} and the complementary strand C^{12} → G^{22}. For the modified strand, the NOE cross-peaks adjacent to the *R,R*-DHB-dA adduct, C^5 H6 → C^5 H1′, C^5 H1′ → R^6 H8, R^6 H8 → R^6 H1′, and R^6 H1′ → A^7 H8 were of similar intensities as compared to the cross-peaks arising from distal nucleotides. For the complementary strand, among the cross-peaks of bases proximal to the DHB-dA adduct, those arising from T^{16}, T^{17}, and G^{18} were of similar intensities compared to the remainder of the cross-peaks from nucleotides distal to the adduct. The greatest chemical shift perturbations as compared to the unmodified-duplex (Figure S1 in the Supporting Information) were observed in the modified strand, for C^5 H5, which shifted 0.1 ppm upfield, C^5 H1′, which shifted 0.3 ppm downfield, R^6 H8, which shifted 0.1 ppm upfield, and R^6 H2, which shifted 0.1 ppm downfield. Minimal chemical shift perturbations were observed for the complementary strand.

Imino Proton Assignments. The sequential pattern of cross-peaks between imino protons[81] was observed for base pairs G^2:C^{21} → G^3:C^{20} → A^4:T^{19} → C^5:G^{18}. The T^{16} N3H → T^{17} N3H and T^{17} N3H → G^{18} N1H sequential cross-peaks were not observed, indicative of structural changes in the vicinity of the adduct. The sequential walk resumed from G^8:C^{15} → A^9:T^{14} → A^{10}:T^{13} (Figure 2, panels A–C). The NOEs between the base imino and amino protons and adenine H2 protons showed cross-peaks for all base pairs, with an exception of the terminal base G^{22} (Figure 2B). The A^7 H2 → T^{16} N3H cross-peak was of lower intensity compared to the other cross-peaks and overlapped with the G^{11} N1H → C^{12} N^2H1 cross-peak. The R^6 H2 → T^{17} N3H cross-peak (k, Figure 2, panel B) was visible when the contour levels of the spectrum were lowered; its intensity was significantly lower than the remainder of the A:T cross-peaks. The greatest chemical shift perturbation was observed for the T^{17} N3H proton, which shifted 0.35 ppm upfield as compared to that of the unmodified-duplex (Figure S2 in the Supporting Information). The T^{16} and T^{17} imino protons resonances (Figure S3 in the Supporting Information) were broader and of lower intensity as compared to that of the unmodified-duplex (Figure S4 in the Supporting Information) at 5 °C, and when the temperature was increased to 20 °C, both resonances disappeared (Figure S3 in the Supporting Information).

R,R-DHB-dA Proton Assignments. The *R,R*-DHB-dA adduct is characterized by a 2-fold rotation axis about the C6-N^6 bond. The pro-*R* and pro-*S* diastereotopic hydrogens on the two methylene groups are symmetry related with respect to rotation about this bond, as are the corresponding hydroxyl and hydrogen substituents on the stereoisomeric carbons of the DHB moiety. Accordingly, the two pro-*R* methylene hydrogens are designated H_{α} and $H_{\alpha'}$, the two methylene pro-*S* hydrogens are designated H_{β} and $H_{\beta'}$, and the stereoisomeric hydrogens on the hydroxylated carbons are designated H_{γ} and $H_{\gamma'}$ (Chart 1). Six resonances were observed between 3.6 and 4.4 ppm (Figure 3A). This indicated that on the NMR time scale, the DHB moiety did not rapidly rotate about the C6-N^6 bond and that the nonsymmetric DNA environment split the three sets of symmetry-related hydrogens into six resonances. This observation was consistent with previous calculations that indicated partial double bond character for the C6-N^6 bond.[56] These resonances were observed in the same region of the spectrum as the resonances for the 1,4-bis(2′-deoxyadenosin-N^6-yl)-2*S*,3*S*-butanediol intrastrand DEB-derived cross-link in the same sequence.[82] For the two sets of methylene protons, i.e., $H_{\alpha,\beta}$ and $H_{\alpha',\beta'}$ (Chart 1), it was not possible to establish unequivocally which was the resonance arising from the pro-*R* hydrogen and which was the resonance arising from the pro-*S*

dx.doi.org/10.1021/tx400472p | *Chem. Res. Toxicol.* 2014, 27, 805–817

hydrogen. However, it was possible to assign the two sets of methylene resonances, based upon NOEs to DNA protons. One set of methylene resonances, assigned as the $H_{\alpha,\beta}$ hydrogens, was located at 3.88 and 3.95 ppm, and the other set, assigned as the $H_{\alpha',\beta'}$ hydrogens, was located at 3.64 and 3.73 ppm. The $H_{\alpha',\beta'}$ set of resonances exhibited a strong NOE to C^5 H5 and weak NOEs to C^5 H6 [not observed at the contour level plotted in Figure 3]. This set of methylene protons exhibited weak NOEs to A^7 H2 in the 3′-direction. These methylene protons exhibited NOEs to the R^6 H2 resonance at 7.27 ppm. They also exhibited strong NOEs to the major groove T^{16} CH_3 protons, located in the 3′-neighbor A^7:T^{16} base pair. The $H_{\alpha,\beta}$ methylene protons exhibited strong NOEs to C^5 H5 and weaker NOEs to C^5 H6. This set of methylene protons did not exhibit NOEs to R^6 H2. The diastereomeric H_γ and $H_{\gamma'}$ protons were identified at 4.31 and 4.29 ppm. It was possible to make the assignments of the H_γ and $H_{\gamma'}$ based on the NOE intensities to the methylene protons. H_γ had stronger cross-peaks to the $H_{\alpha,\beta}$ and weaker cross-peaks to $H_{\alpha',\beta'}$. The opposite results were observed for $H_{\gamma'}$, which exhibited stronger cross-peaks to $H_{\alpha',\beta'}$ and weaker to $H_{\alpha,\beta}$. NOEs were observed from both to the neighbor base A^7 H2, C^5 H6, C^5 H5, and T^{16} CH_3 protons. Weak interstrand NOEs were observed between $H_{\alpha,\alpha'}$, $H_{\beta,\beta'}$ and $H_{\gamma,\gamma'}$ of R^6 and the imino proton of G^{18} (Figure 2, panel A).

Structural Refinement of the *R,R*-DHB-dA Duplex. A total of 204 distance restraints obtained from the analyses of the NOESY spectra of nonexchangeable protons were used for restrained molecular dynamics (rMD) calculations, where 106 were internucleotide restraints and 98 were intranucleotide restraints. The average well width for the distance of the upper and lower bounds was 1.5 Å. A simulated annealing protocol was used. A total of 90 empirical backbone torsion angles, 42 empirical hydrogen bonding, and 17 empirical deoxyribose pseudorotations were included as experimental restraints in the calculations (Table 1). These were included based upon the observation that with the exception of the modified base pair R^6:T^{17}, and the neighboring base pairs C^5:G^{18} and A^7:T^{16}, the remainder of the NMR data were consistent with a right-handed helical DNA-duplex similar to the canonical B-form DNA.[70] The distereotopic $H_{\alpha,\beta}$ and $H_{\alpha',\beta'}$ protons of the DHB group could not be assigned unequivocally. In several instances, however, both exhibited similar NOE cross-peak intensities to specific DNA protons. Such distances were included in the rMD calculations. Additionally, several NOEs involving the exchangeable protons overlapped, precluding accurate distance calculations, so distances involving these exchangeable protons were not included in the rMD calculations. Table 1 summarizes the restraints that were used and the refinement statistics.

Eight structures emergent from the rMD calculations were subjected to potential energy minimization. Figure S5, panel A of the Supporting Information shows these eight superimposed structures. Good convergence was observed, with a maximum pairwise rmsd between the eight structures of 0.67 Å (Table 2).

Table 1. NMR Restraints Used for the rMD Structural Refinement of the *R,R*- and *S,S*-Duplexes, and the Refinement Statistics

NMR restraints	*R,R*-duplex	*S,S*-duplex
NOE restraints		
internucleotide	106	103
intranucleotide	98	96
total	204	199
backbone torsion angle restraints	90	90
hydrogen bonding restraints	42	42
deoxyribose pseudorotation restraints	17	17
total number of restraints	353	348
refinement statistics		
number of distance restraint violations >0.025 Å	8	10
number of torsion restraint violations	8	7
total distance penalty/maximum penalty [kcal mol^{-1}]	0.48/0.11	0.82/0.31
total torsion penalty/maximum penalty [kcal mol^{-1}]	0.59/0.13	3.15/1.61
r.m.s. distances (Å)	0.012	0.012
r.m.s. angles (deg)	2.32	2.30
distance restraint force constant [kcal mol^{-1} $Å^{-2}$]	32	32
torsion restraint force constant [kcal mol^{-1} deg^{-2}]	32	32
average well width for distance restraints [Å]	1.5	1.5

Table 2. Structural Statistics for the *R,R*- and *S,S*-Duplexes

average structure (obtained from 8 structures)	*R,R*-duplex	*S,S*-duplex
RMS pairwise difference between structures [Å]	0.67	0.66
RMS difference from average structure [Å]	0.45	0.44
CORMA analysis for average structure[a] R_1^{x}[b]		
intranucleotide	0.068	0.071
internucleotide	0.080	0.086
total	0.074	0.078
average error[c]	0.016	0.016

[a]The mixing time was 250 ms. [b]R_1^{x} is the sixth root R factor: $\Sigma[((I_o)_i^{1/6}) - ((I_c)_i^{1/6})/\Sigma((I_o)_i^{1/6})]$. [c]Average error: $\Sigma(I_c - I_o)/n$, where I_c values are NOE intensities calculated from refined structure, and I_o values are experimental NOE intensities.

These eight structures were averaged, and the resulting average structure was subjected to complete relaxation matrix analysis.[67] The results are shown in Figure 4A. In general, the sixth root residuals (R_1^{x} values) were consistently below 10%, for both intranucleotide NOEs and internucleotide NOEs. This indicated that the average of the refined structures was in reasonable agreement with the experimental NOE intensities. Base pairs A^{10}:T^{13} and G^{11}:C^{12}, located at the 3′-end of the duplex with respect to R^6, showed somewhat poorer agreement with the experimental NOE intensities. This was attributed to a combination of spectral overlap and increased fraying of the duplex at this end. Table 2 summarizes the structural statistics.

Figure 5A shows the average structure of the *R,R*-duplex in the region of the C^5:G^{18}, R^6:T^{17} and A^7:T^{16} base pairs. The view is from the major groove. The *R,R*-DHB-dA nucleoside maintained the anti conformation about the glycosyl bond, and the adduct was located in the major groove. The DHB moiety rotated around the C6-N^6 bond such that the diastereotopic R^6 $H_{\alpha,\beta}$ hydrogens were oriented toward the 5′ direction and were in proximity to the major groove edge of the C^5 base. This placed the diastereotopic R^6 $H_{\alpha',\beta'}$ hydrogens in the 3′ direction, facing toward base pair A^7:T^{16}. The stereoisomeric hydroxyls of the *R,R*-DHB moiety both faced into the major groove. They did not participate in hydrogen bonding interactions with the DNA. With respect to base pairing, the R^6 base was positioned such that it could maintain only one Watson−Crick hydrogen bond with the complementary thymine T^{17}, between the N1 imine nitrogen and the T^{17} N3H imino proton (Figure S6 in the Supporting

dx.doi.org/10.1021/tx400472p | Chem. Res. Toxicol. 2014, 27, 805−817

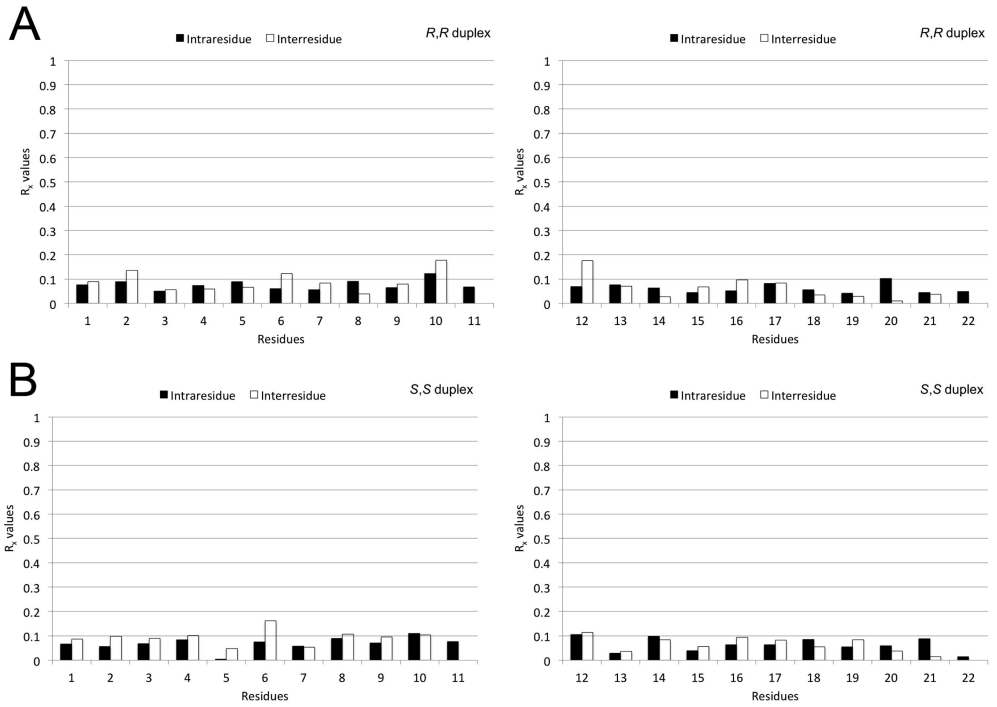

Figure 4. Complete relaxation matrix analysis results for internucleotide and intranucleotide NOEs for the *R,R*- and *S,S*-DHB-dA duplexes. (A) The *R,R*-DHB-dA duplex. (B) The *S,S*-DHB-dA duplex. R_1^x is the sixth root *R* factor: $\Sigma[((I_o)_i^{1/6}) - ((I_c)_i^{1/6})/\Sigma((I_o)_i^{1/6})]$, where I_c values are NOE intensities calculated from the refined structure, and I_o values are experimental NOE intensities.

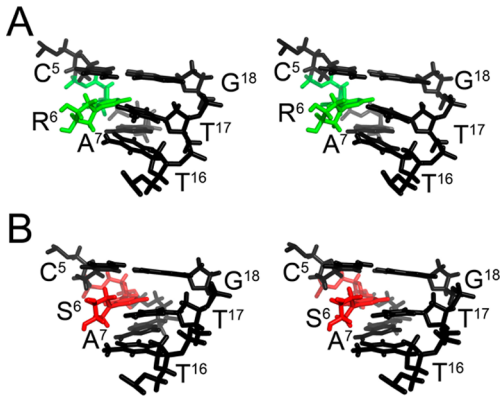

Figure 5. Average structures of the *R,R*- and *S,S*-DHB-dA modified duplexes. (A) Stereo drawing for the *R,R*-DHB-dA duplex in the region of the C^5:G^{18}, R^6:T^{17}, and A^7:T^{16} base pairs. (B) Stereo drawing for the *S,S*-DHB-dA duplex in the region of the C^5:G^{18}, S^6:T^{17}, and A^7:T^{16} base pairs. The modified nucleotides R^6 or S^6 are shown in green and red, respectively.

Information). The distance between R^6 N1 and T^{17} N3H was 2.1 Å, and the distance between A^7 N1 and T^{16} N3H was 2.0 Å, which was slightly longer than that for an unmodified A:T base pair, which is typically 1.9 Å. This was confirmed by helicoidal analysis,[78] where the opening parameter for the R^6:T^{17} base pair was 19° (Figure S7 in the Supporting Information) but was 6° for the unmodified duplex.[55] The modified R^6 base was tilted out of plane, as was also discerned by helicoidal analysis (Figure S8 in the Supporting Information). The exocyclic DHB ring of the R^6 base was rotated out of plane and the N1-C6-N^6-C_δ dihedral angle was −118°. Watson−Crick base pairing geometry at the neighboring C^5:G^{18} and A^7:T^{16} base pairs was maintained. However, the A^7:T^{16} base pair exhibited lower stability as could be observed from NMR data collected as a function of temperature (Figure S3 of the Supporting Information). The *R,R*-DHB-dA adduct perturbed stacking interactions at base pairs C^5:G^{18}, R^6:T^{17}, and A^7:T^{16} (Figure 6A,B) Thus, R^6 stacked with its 5′ neighbor C^5 but not with its 3′ neighbor A^7. The complementary thymine T^{17} stacked well with its 5′ neighbor T^{16} but not with 3′ neighbor G^{18}.

NMR Spectroscopy of the *S,S*-DHB-dA Duplex. *Base Proton Assignments.* The region of the NOESY spectrum showing the resonances between aromatic protons of the bases to the deoxyribose H1′ protons[79,80] for the modified strand C^1

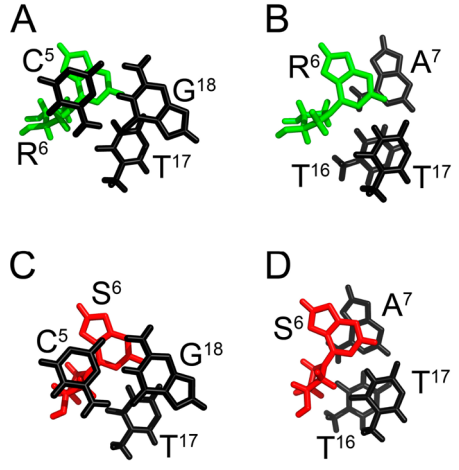

Figure 6. Stacking interactions for the *R,R*- and *S,S*-DHB-dA duplexes. (A) The *R,R*-DHB-dA duplex. Stacking of the C^5:G^{18} base pair (black) above R^6 (green) and T^{17} (black). (B) The *S,S*-DHB-dA duplex. Stacking of the R^6:T^{17} pair (in green and black, respectively) above the base pair A^7:T^{16} (black). (C) Stacking of the C^5:G^{18} base pair (black) above S^6 (red) and T^{17} (black). (D) Stacking of the S^6:T^{17} pair (in red and black, respectively) above the base pair A^7:T^{16} (black).

dx.doi.org/10.1021/tx400472p | *Chem. Res. Toxicol.* 2014, 27, 805−817

→ G^{11} and for the complementary strand C^{12} → G^{22} is shown in Figure 1C,D. For the modified strand, the sequential NOE cross-peaks C^5 H6 → C^5 H1′, C^5 H1′ → S^6 H8, S^6 H8 → S^6 H1′, and S^6 H1′ → A^7 H8 were of similar intensities compared to those of the other cross-peaks arising from nucleotides distal to the adduct. Likewise, for the complementary strand, the sequential NOE cross-peaks for the bases proximal to the adduct T^{16} H6 → T^{16} H1′, T^{16} H1′ → T^{17} H6, T^{17} H6 → T^{17} H1′, and T^{17} H1′ → G^{18} H8 were of similar intensities as compared to the remainder of the cross-peaks arising from bases distal to the adduct. The greatest chemical shift perturbations compared to the unmodified duplex (Figure S1 of the Supporting Information) were observed for C^5 H5, which shifted upfield 0.1 ppm, C^5 H1′, which shifted downfield 0.3 ppm, S^6 H8, which shifted upfield 0.1 ppm, and S^6 H2, which shifted downfield 0.1 ppm. Minimal chemical shift perturbations were observed for the complementary strand.

Imino Proton Assignments. Figure 2 D−F shows an expansion of the NOESY spectrum, in the far downfield region in which the Watson−Crick base paired imino proton resonances are visible. The sequential NOE cross-peaks between imino protons[81] were observed for base pairs G^2:C^{21} → G^3:C^{20} → A^4:T^{19} → C^5:G^{18}. The sequential NOE cross-peaks between imino protons for base pairs C^5:G^{18} → S^6:T^{17} and S^6:T^{17} → A^7:T^{16} were not observed. The sequential pattern of NOE cross-peaks could be continued from G^8:C^{15} → A^9:T^{14} → A^{10}:T^{13} (Figure 2, panel F). The region of the spectrum showing NOEs between the base imino and the amino and adenine H2 protons exhibited the anticipated NOE cross-peaks for all base pairs, except for the terminal base G^{22} (Figure 2, panel E). The S^6 H2 → T^{17} N3H cross-peak (g, Figure 2, panel E) was visible when the contour level of the spectrum was lowered and overlapped with the G^{11} N1H → C^{12} N^2 H1 cross-peak; its intensity was significantly lower than the remainder of the A:T cross-peaks. The A^7 H2 → T^{16} N3H cross-peak was of lower intensity as compared to the other cross-peaks. The greatest chemical shift perturbation was observed for the T^{17} N3H resonance, which moved 0.35 ppm upfield as compared to the unmodified duplex (Figure S2 of the Supporting Information). The intensities of the T^{16} N3H and T^{17} N3H resonances were significantly lower (Figure S9 in the Supporting Information). These resonances were broader compared to their counterparts in the unmodified duplex (Figure S4 of the Supporting Information). Both resonances disappeared from the spectrum when the experiment was conducted at 20 °C.

S,S-DHB-dA Proton Assignments. Six *S,S*-DHB-dA adduct resonances were observed between 3.62 and 4.36 ppm (Figure 3B). This indicated that on the NMR time scale the DHB moiety did not rapidly rotate about the C6-N^6 bond. Two sets of diastereotopic methylene proton resonances, i.e., $H_{\alpha,\beta}$ and $H_{\alpha',\beta'}$ (Chart 1), were identified, one located at 3.62 and 3.70 ppm and the other at 3.66 and 4.14 ppm. It was not possible to establish unequivocally which resonances were arising from the pro-*R* and from the pro-*S* hydrogen. It was possible to assign the two sets of methylene resonances, based upon NOEs to DNA protons. The set of methylene resonances at 3.66 and 4.14 ppm, assigned as the $H_{\alpha,\beta}$ hydrogens, exhibited intense NOEs to C^5 H5 of the 5′-neighbor C^5:G^{18} base pair at 5.14 ppm. They exhibited weaker NOEs to C^5 H6. The set of methylene resonances at 3.62 and 3.70 ppm, assigned as the $H_{\alpha',\beta'}$ protons, exhibited NOEs to S^6 H2 and a weak NOE to A^7 H2. They also exhibited NOEs to the T^{16} CH_3 protons at 1.69 ppm. The diastereomeric protons H_γ and $H_{\gamma'}$ were identified at 4.36 ppm and 4.25 ppm. The resonance at 4.36 ppm showed stronger NOEs to the $H_{\alpha,\beta}$ protons, whereas the resonance at 4.25 ppm exhibited NOEs to the $H_{\alpha',\beta'}$ protons. The $H_{\alpha',\beta'}$ protons gave more intense cross-peaks to the S^6 H2 compared to that of other adduct protons. Additional weak interstrand cross-peaks were observed between the adduct protons S^6 $H_{\alpha',\beta'}$ and $H_{\alpha,\beta}$ and the G^{18} N1H imino proton (cross-peaks a and b, Figure 2, panel D).

Structural Refinement of the *S,S*-DHB-dA Duplex. The structure of the *S,S*-duplex was determined using a simulated annealing rMD protocol, using distance restraints determined from the NOE data. A total of 199 NOE-based distance restraints were employed, which included 103 internucleotide restraints and 96 internucleotide restraints (Table 1). The diastereotopic DHB $H_{\alpha,\beta}$ and $H_{\alpha',\beta'}$ proton resonances could not be unequivocally assigned. As for the *R,R*-DHB-dA adduct, in some instances these protons exhibited similar NOE intensities to specific DNA protons, and in such cases, it was possible to include these distances in the rMD calculations. Also, the weak interstrand cross-peaks between DHB $H_{\alpha,\beta}$ and $H_{\alpha',\beta'}$ protons and the G^{18} N1H imino proton were not included in the structure calculations. The experimentally determined restraints were supplemented with 90 empirical phosphodiester backbone restraints, 42 Watson−Crick hydrogen bonding restraints, and 17 deoxyribose pseudorotation restraints. The inclusion of these empirical restraints was predicated upon the observation that the NMR data suggested that apart from the modified base pair S^6:T^{17} and its 5′- and 3′-neighboring base pairs C^5:G^{18} and A^7:T^{16}, the duplex maintained a right handed B-DNA-like conformation in solution. Table 1 shows the restraints used for rMD calculations. Eight structures that emerged from the rMD calculations were subjected to potential energy minimization. These are shown superimposed in Figure S5, panel B of the Supporting Information. These structures converged to a maximum pairwise rmsd value of 0.66 Å and were used to calculate an average structure, which was subjected to complete relaxation matrix analysis.[67] The overall sixth root residual (R_1^x) was 7.8% (Table 2). An evaluation of the R_1^x residuals for individual nucleotides (Figure 4B) indicated that these were consistently within the 10% range. Thus, the average structure was in good agreement with the observed NOE intensities. Table 1 shows the structural statistics.

Figure 5B shows the *S,S*-duplex in the region of the C^5:G^{18}, S^6:T^{17}, and A^7:T^{16} base pairs, viewed from the major groove. The *S,S*-DHB-dA modified base adopted the anti conformation about the glycosyl bond. The DHB moiety was located in the major groove. The adduct rotated around the C6-N^6 bond and was positioned such that the S^6 $H_{\alpha,\beta}$ hydrogens oriented toward the 5′ direction and were proximate to the C^5 base. This placed the S^6 $H_{\alpha',\beta'}$ hydrogens toward the 3′-neighbor A^7:T^{16} base pair. The stereoisomeric hydroxyl groups of the DHB moiety both faced into the major groove, and they did not form hydrogen bonds with the DNA. The H_γ proton faced toward the modified strand, whereas the $H_{\gamma'}$ proton faced toward the complementary strand. The S^6 base formed one Watson−Crick hydrogen bond between the S^6 N1 imine nitrogen and the T^{17} imino proton (Figure S10 in the Supporting Information). The distance between S^6 N1 and N3H was 2.0 Å, which is slightly longer than that for an unmodified A:T base pair, which is typically 1.9 Å. It is also confirmed by helicoidal analysis, where the opening for the S^6:T^{17} base pair was 12° higher than that

dx.doi.org/10.1021/tx400472p | *Chem. Res. Toxicol.* 2014, 27, 805−817

for other base pairs (Figure S7 of the Supporting Information). The exocyclic DHB ring of the S^6 base was rotated out of plane, and the N1-C6-N^6-C_δ dihedral angle was −123°. Watson−Crick hydrogen bonding at the neighbor base pairs was maintained. However, the A^7:T^{16} base pair exhibited lower stability as observed in the NMR spectra obtained as a function of temperature (Figure S9 of the Supporting Information). The *S,S*-DHB-dA base interfered with base stacking interactions. It did not stack well with its 5′ neighbor C^5 but stacked well with its 3′ neighbor A^7 (Figure 6C,D. The complementary thymine T^{17} did stack well with its 5′ neighbor T^{16} but not with 3′ neighbor G^{18}.

DISCUSSION

The potential for bis-alkylation of DNA appears to be critical for the mutagenicity and cytotoxicity of DEB,[83] as butadiene mono-oxidation products, e.g., EB and EBD, are much less genotoxic.[44] Adenine adducts are likely to play a major role in the genotoxicity of DEB since the number of A:T base pair substitutions equals or exceeds the number of mutations at the G:C base pairs,[84] despite the fact that DEB preferentially alkylates guanines in DNA.[83] Thus, one or more DEB-specific dA lesions must contribute to DEB-induced genotoxicity.[53,84,85] However, the specific DEB-dA adducts capable of inducing these A to T transversions remain obscure.[53,86,87] The double alkylation of the *R,R*- and *S,S*-DHB-dA adducts removes the N^6-dA amino groups as hydrogen bond donors in base pairing with dT and raises the question as to how the bulky 3,4-dihydroxypyrrolidine rings are accommodated in the DNA duplex. UV melting studies have revealed that the *R,R*- and *S,S*-DHB-dA adducts significantly destabilize duplex DNA, evidenced by a 16−17 °C decrease in T_m as compared to that of unmodified DNA.[56] However, CD studies have suggested that *R,R*- and *S,S*-DHB-dA-modfied DNA duplexes maintain a B-type DNA conformation.[56] Consequently, it was of interest to determine the solution structures of the *R,R*- and *S,S*-DHB-dA adducts.

Structures of the *R,R*- and *S,S*-DHB-dA Adducts. The structures of the *R,R*- and *S,S*-DHB-dA adducts in DNA are similar, and both adducts are positioned in the major groove of DNA. In both instances, the bulky 3,4-dihydroxypyrrolidine rings are accommodated by an out-of-plane rotation about the C6-N^6 bond of the bis-alkylated adenine such that the $H_{\alpha,\beta}$ protons orient in the 5′-direction, whereas the $H_{\alpha',\beta'}$ protons orient in the 3′-direction. In both instances, this directionality of the 3,4-dihydroxypyrrolidine ring is evidenced by the patterns of NOEs between 3,4-dihydroxypyrrolidine protons and DNA. For the *R,R*-DHB-dA adduct, NOEs between the $H_{\alpha,\beta}$ protons and C^5 H5 (Figure 3A) confirm that the $H_{\alpha,\beta}$ protons orient in the 5′ direction and are proximate to the C^5 base. The largest downfield chemical shift of 0.3 ppm compared to that of the unmodified duplex is observed for C^5 H1′, which is attributed to a less planar stacking of the C^5 and Y^6 bases. Likewise, for the *S,S*-DHB-dA adduct, similar NOEs are observed between $H_{\alpha,\beta}$ protons and C^5 H5 (Figure 3B). The conclusion that both the *R,R*- and *S,S*-DHB-dA modified bases maintain the anti conformation about the glycosyl bond is supported by the intensities of the R^6 H8 → R^6 H1′ and S^6 H8 → S^6 H1′ NOEs, which are similar to those of the other nucleobase aromatic proton → deoxyribose H1′ NOEs (Figure 1). In both instances, maintaining the anti conformation of the glycosyl bond, combined with the out-of-plane rotation about the C6-N^6 bond, allows the complementary thymine, T^{17}, to remain stacked within the duplex and form one hydrogen bond with the modified base pair, between the imine nitrogen of the modified base and the T^{17} N3H imino proton. For the *R,R*-DHB-dA adduct, the presence of this hydrogen bond is revealed by the weak NOE between R^6 H2 and T^{17} N3H (cross-peak k, Figure 2, panel B). Likewise, the presence of the corresponding hydrogen bond at the modified S^6:T^{17} base pair is indicated by the weak NOE between S^6 H2 and T^{17} N3H (cross-peak g, Figure 2, panel E). The loss of the second Watson−Crick hydrogen bonding interaction at the lesion sites correlates with the significantly lower thermal stabilities of the *R,R*- and *S,S*-DHB-dA duplexes, as compared to that of the unmodified duplex. The reduced base stacking at the adduct sites may also contribute to the thermal destabilization. In particular, both the R^6 and S^6 bases stack with the 5′ neighbor C^5 but not with the 3′ neighbor A^7 (Figure 6). Likewise, in both instances, the complementary thymine T^{17} stacks well with the 5′ neighbor T^{16} but not with the 3′ neighbor G^{18}.

In summary, these data suggest that out-of-plane rotations of the 3,4-dihydroxypyrrolidine rings allow the complementary thymine to be accommodated in the DNA duplex. Density functional calculations at the nucleoside level have revealed that the pyrrolidine nitrogen lone electron pair is shared with the π-electron system of the purine ring, resulting in partial double bond character and a barrier to rotation about the C6-N^6 bond.[56] At the nucleoside level, the two sets of methylene protons for the pyrrolidine ring experience different chemical shift environments. The same is observed in duplex DNA (vide infra). Hence, the rMD calculations employed herein utilized an sp^2 hybridized pyrrolidine nitrogen. These calculations suggest that the adenine C6-N^6 bond possesses sufficient single bond character to facilitate its out-of-plane orientation with respect to the adenine nucleobase. Accordingly, a second set of rMD calculations was performed, which utilized an sp^3 hybridized pyrrolidine nitrogen. The resulting structures were similar, with the pyrrolidine rings of both DHB-dA stereoisomers similarly orienting in the major groove. Complete relaxation matrix calculations performed on the refined structures emergent from the calculations involving the sp^3 hybridized pyrrolidine nitrogen showed comparable agreement with the NOESY data at the modified base pairs, as was obtained from the refined structures involving the sp^2 hybridized pyrrolidine nitrogen. Overall, this is consistent with the conclusion that the adenine C6-N^6 bond possesses some degree of partial double bond character but retains sufficient single bond character to allow the 3,4-dihydroxypyrrolidine ring to rotate out of the plane of the adenine nucleobase.

While both the *R,R*- and *S,S*-DHB-dA adducts are oriented in the major groove, they differ as to the configurations of the hydroxyl groups at the stereoisomeric carbon atoms of the 3,4-dihydroxypyrrolidine ring. It was thus of interest to examine the possibility of differential hydrogen bonding patterns between the stereoisomeric hydroxyl groups and the DNA. However, the structural data does not support the notion that the *R,R*- and *S,S*-DHB-dA adducts exhibit differential hydrogen bonding patterns between the stereoisomeric hydroxyls and the DNA. Also, the thermodynamic data do not suggest the formation of interstrand hydrogen bonding interactions by these stereoisomeric lesions. In both instances, the DNA is destabilized, and for *R,R*-duplex, T_m is 28°, while for the *S,S*-duplex, T_m is 27°. This suggests that neither modified duplex is stabilized by hydrogen bonding interactions involving the DHB hydroxyl

groups. However, differential orientations of the DHB hydroxyl groups might provide a mechanism to differentially interact with DNA polymerases during translesion bypass, thus modulating mutagenic outcomes. Consequently, it will be of interest to examine the structures of the *R,R*- and *S,S*-DHB-dA adducts in the context of translesion replication complexes.

Structure–Activity Relationships. The orientations of the *R,R*- and *S,S*-DHB-dA adducts in the major groove of DNA with respect to the bis-alkylated adenine nucleobase allows for thymine in the complementary strand to be accommodated in the DNA duplex with relatively little distortion. However, because the pyrrolidine nitrogen cannot participate in hydrogen bonding with thymine in the complementary strand, at the DNA damage site, the damaged DNA base pair is stabilized by a single hydrogen bond. Thus, the loss of the T O^4 → A N^6H Watson–Crick hydrogen bond, coupled with reduced base stacking interactions, probably accounts for the significant decrease in T_m observed for both the *R,R*- and *S,S*-DHB-dA adducts. Structural studies of a series of other monodentate N^6-dA adducts arising from styrene oxide and butadiene epoxides suggest that they also are contained within the major groove but induce less structural perturbation of Watson–Crick base pairing in DNA.[88−93] Repair mechanisms responsible for the removal of the *R,R*- and *S,S*-DHB-dA lesions in cells are currently under investigation. Our initial results using extracts from human fibrosarcoma (HT1080) cells suggest that DHB-dA is rapidly repaired.[94] Site-specific mutagenesis studies conducted in *E. coli* have revealed that the *R,R*- and *S,S*-DHB-dA adducts are weakly mutagenic,[95] which could potentially be due to the efficient repair of these adducts in vivo. However, our replication studies in vitro have revealed that DHB-dA is bypassed in an error-prone manner by human translesion synthesis (TLS) polymerases κ and η. These studies suggest that DHB-dA adducts can induce both base substitution and deletion mutations (Kotapati and Tretyakova, unpublished results).[96]

Summary. Both *R,R*- and *S,S*- stereoisomers of DEB-induced N^6,N^6-DHB-dA adducts are oriented in the major groove of DNA. For both adducts, this allows thymine in the complementary strand of the DNA to be inserted into the duplex. However, the complementary thymine forms only a single hydrogen bond with the damaged adenine due to the fact that the N^6-protons of the modified bases are replaced by the pyrrolidine ring, which cannot participate in hydrogen bonding with the complementary thymine. Moreover, the complementary thymine is displaced toward the DNA minor groove, weakening its stacking interactions with the neighboring base pairs. This may explain the thermal destabilization induced into DNA by the *R,R*- and *S,S*-DHB-dA adducts and predicts that they might be good candidates for base excision repair. The structural data do not support the notion that the *R,R*- and *S,S*-DHB-dA adducts show differential hydrogen bonding patterns with the complementary strand involving the stereoisomeric pyrrolidine ring hydroxyl groups.

■ ASSOCIATED CONTENT

Supporting Information

Parameter files for the *R,R* and *S,S* adducts used for AMBER calculations; chemical shift table of the nonexchangeable protons for the *R,R*- and *S,S*-duplexes; chemical shift table of the exchangeable imino and amino protons for the *R,R*- and *S,S*-duplexes; NOESY spectrum of the unmodified duplex, showing sequential NOEs between the aromatic and anomeric protons; NOESY spectrum for the unmodified duplex in H_2O; NMR spectra showing the imino proton resonances for the *R,R*-DHB-dA duplex as a function of temperature; NMR spectra showing the imino proton resonances for the unmodified duplex as a function of temperature; superpositions of eight structures obtained from rMD calculations for the *R,R*- and *S,S*-duplexes; the R^6:T^{17} base pair, in the *R,R*-duplex; helicoidal analysis for the *R,R*- and *S,S*-duplexes; NMR spectra showing the imino proton resonances for the *S,S*-DHB-dA duplex as a function of temperature; and the S^6:T^{17} base pair in the *S,S*-duplex. This material is available free of charge via the Internet at http://pubs.acs.org.

■ AUTHOR INFORMATION

Corresponding Author

*Tel: 615-322-2589. Fax: 615-322-7591. E-mail michael.p.stone@vanderbilt.edu.

Funding

This work was supported by NIH grants R01 ES-05509 (to M.P.S.) and CA-100670 (to N.T.). The Vanderbilt University Center in Molecular Toxicology is supported by NIH grant P30 ES-00267. Funding for NMR was supplied by NIH grants S10 RR-05805 and S10 RR-025677 and NSF grant DBI 0922862, the latter funded by the American Recovery and Reinvestment Act of 2009 (Public Law 111-5). Vanderbilt University assisted with the purchase of NMR instrumentation.

Notes

Portions of this work were presented at the 242nd National Meeting of the American Chemical Society, Denver, CO.[97]
The authors declare no competing financial interest.

■ ABBREVIATIONS

BD, 1,3-butadiene; dA, 2′-deoxyadenosine; DIPEA, *N,N*-diisopropylethyl amine; DMSO, dimethylsulfoxide; DMTr, 4,4′-dimethoxytrityl; dR, 2′-deoxyribose; EB, 1,2-epoxy-3-butene; DEB, 1,2,3,4-diepoxybutane; EBD, 1,2-dihydroxy-3,4-epoxybutane; *R,R*-DHB-dA, *R,R*-N^6,N^6-(2,3-dihydroxybutan-1,4-diyl)-2′-deoxyadenosine; *S,S*-DHB-dA, *S,S*-N^6,N^6-(2,3-dihydroxybutan-1,4-diyl)-2′-deoxyadenosine; LC–ESI–MS, liquid chromatography–electrospray ionization–mass spectrometry; R_1^x, sixth root residual; rMD, restrained molecular dynamics; rmsd, root-mean-square deviation; SBR, styrene-butadiene rubber; NOESY, Nuclear Overhauser effect spectroscopy; CD, circular dichroism; DQF-COSY, double quantum filtered correlated spectroscopy; HPLC, high-performance liquid chromatography

■ REFERENCES

(1) Himmelstein, M. W., Acquavella, J. F., Recio, L., Medinsky, M. A., and Bond, J. A. (1997) Toxicology and epidemiology of 1,3-butadiene. *Crit. Rev. Toxicol. 27*, 1–108.

(2) Jackson, M. A., Stack, H. F., Rice, J. M., and Waters, M. D. (2000) A review of the genetic and related effects of 1,3-butadiene in rodents and humans. *Mutat. Res. 463*, 181–213.

(3) Pelz, N., Dempster, N. M., and Shore, P. R. (1990) Analysis of low molecular weight hydrocarbons including 1,3-butadiene in engine exhaust gases using an aluminum oxide porous-layer open-tubular fused-silica column. *J. Chromatogr. Sci. 28*, 230–235.

(4) Brunnemann, K. D., Kagan, M. R., Cox, J. E., and Hoffmann, D. (1990) Analysis of 1,3-butadiene and other selected gas-phase components in cigarette mainstream and sidestream smoke by gas chromatography-mass selective detection. *Carcinogenesis 11*, 1863–1868.

(5) National Toxicology Program (NTP) (1984) Toxicology and Carcinogenesis Studies of 1,3-Butadiene (CAS No. 106-99-0) in B6c3F1 Mice (Inhalation Studies), *Technical Report Series 288*, NIH Publication no. 84-2544, pp 111, National Toxicology Program, Research Triangle Park, NC. http://ntp.niehs.nih.gov/ntp/htdocs/LT_rpts/tr288.pdf
(6) National Toxicology Program (NTP) (1993) National Toxicology Program Toxicology and Carcinogenesis Studies of 1,3-Butadiene (CAS No. 106-99-0) in B6c3F1 Mice (Inhalation Studies), *Technical Report Series 434*, NIH Publication no. 93-3165, pp 391, National Toxicology Program, Research Triangle Park, NC. http://ntp.niehs.nih.gov/ntp/htdocs/LT_rpts/tr434.pdf
(7) Huff, J. E., Melnick, R. L., Solleveld, H. A., Haseman, J. K., Powers, M., and Miller, R. A. (1985) Multiple organ carcinogenicity of 1,3-butadiene in B6c3F1 mice after 60 weeks of inhalation exposure. *Science 227*, 548−549.
(8) Melnick, R. L., Huff, J., Chou, B. J., and Miller, R. A. (1990) Carcinogenicity of 1,3-butadiene in C57BL/6 x C3H F1 mice at low exposure concentrations. *Cancer Res. 50*, 6592−6599.
(9) Melnick, R. L., Huff, J. E., Roycroft, J. H., Chou, B. J., and Miller, R. A. (1990) Inhalation toxicology and carcinogenicity of 1,3-butadiene in B6c3F1 mice following 65 weeks of exposure. *Environ. Health Perspect. 86*, 27−36.
(10) Owen, P. E., Glaister, J. R., Gaunt, I. F., and Pullinger, D. H. (1987) Inhalation toxicity studies with 1,3-butadiene. 3. Two year toxicity/carcinogenicity study in rats. *Am. Ind. Hyg. Assoc. J. 48*, 407−413.
(11) Owen, P. E., and Glaister, J. R. (1990) Inhalation toxicity and carcinogenicity of 1,3-butadiene in Sprague-Dawley rats. *Environ. Health Perspect. 86*, 19−25.
(12) Csanady, G. A., Guengerich, F. P., and Bond, J. A. (1992) Comparison of the biotransformation of 1,3-butadiene and its metabolite, butadiene monoepoxide, by hepatic and pulmonary tissues from humans, rats and mice. *Carcinogenesis 13*, 1143−1153 [published erratum appears in (1993) *Carcinogenesis 14*, 784].
(13) Henderson, R. F., Barr, E. B., Belinsky, S. A., Benson, J. M., Hahn, F. F., and Menache, M. G. (2000) 1,3-butadiene: cancer, mutations, and adducts. Part I: Carcinogenicity of 1,2,3,4-diepoxybutane. *Res. Rep. Health Eff. Inst.*, 11−43 discussion 45−48.
(14) Henderson, R. F., Thornton-Manning, J. R., Bechtold, W. E., and Dahl, A. R. (1996) Metabolism of 1,3-butadiene: species differences. *Toxicology 113*, 17−22.
(15) Matanoski, G. M., and Schwarts, L. (1987) Mortality of workers in styrene-butadiene polymer production. *J. Occup. Med. 29*, 675−680.
(16) Divine, B. J. (1990) An update on mortality among workers at a 1,3-butadiene facility–preliminary results. *Environ. Health Perspect. 86*, 119−128.
(17) Matanoski, G. M., Santos-Burgoa, C., and Schwartz, L. (1990) Mortality of a cohort of workers in the styrene-butadiene polymer manufacturing industry (1943−1982). *Environ. Health Perspect. 86*, 107−117.
(18) Cole, P., Delzell, E., and Acquavella, J. (1993) Exposure to butadiene and lymphatic and hematopoietic cancer. *Epidemiology 4*, 96−103.
(19) Divine, B. J., and Hartman, C. M. (1996) Mortality update of butadiene production workers. *Toxicology 113*, 169−181.
(20) Matanoski, G., Elliott, E., Tao, X., Francis, M., Correa-Villasenor, A., and Santos-Burgoa, C. (1997) Lymphohematopoietic cancers and butadiene and styrene exposure in synthetic rubber manufacture. *Ann. N.Y. Acad. Sci. 837*, 157−169.
(21) Straif, K., Weiland, S. K., Werner, B., Chambless, L., Mundt, K. A., and Keil, U. (1998) Workplace risk factors for cancer in the German rubber industry: Part 2. Mortality from non-respiratory cancers. *Occup. Environ. Med. 55*, 325−332.
(22) Divine, B. J., and Hartman, C. M. (2001) A cohort mortality study among workers at a 1,3 butadiene facility. *Chem.-Biol. Interact. 135−136*, 535−553.
(23) Graff, J. J., Sathiakumar, N., Macaluso, M., Maldonado, G., Matthews, R., and Delzell, E. (2005) Chemical exposures in the synthetic rubber industry and lymphohematopoietic cancer mortality. *J. Occup. Environ. Med. 47*, 916−932.
(24) Sathiakumar, N., Graff, J., Macaluso, M., Maldonado, G., Matthews, R., and Delzell, E. (2005) An updated study of mortality among North American synthetic rubber industry workers. *Occup. Environ. Med. 62*, 822−829.
(25) Delzell, E., Sathiakumar, N., Graff, J., Macaluso, M., Maldonado, G., and Matthews, R. (2006) An updated study of mortality among North American synthetic rubber industry workers. *Res. Rep. Health Eff. Inst. 132*, 1−63 discussion 65−74..
(26) Sielken, R. L., Jr., Valdez-Flores, C., Gargas, M. L., Kirman, C. R., Teta, M. J., and Delzell, E. (2007) Cancer risk assessment for 1,3-butadiene: Dose-response modeling from an epidemiological perspective. *Chem.-Biol. Interact. 166*, 140−149.
(27) Cheng, H., Sathiakumar, N., Graff, J., Matthews, R., and Delzell, E. (2007) 1,3-Butadiene and leukemia among synthetic rubber industry workers: Exposure-response relationships. *Chem.-Biol. Interact. 166*, 15−24.
(28) Clapp, R. W., Jacobs, M. M., and Loechler, E. L. (2008) Environmental and occupational causes of cancer: New evidence 2005−2007. *Rev. Environ. Health 23*, 1−37.
(29) Whitworth, K. W., Symanski, E., and Coker, A. L. (2008) Childhood lymphohematopoietic cancer incidence and hazardous air pollutants in southeast Texas, 1995−2004. *Environ. Health Perspect. 116*, 1576−1580.
(30) Albertini, R. J., Carson, M. L., Kirman, C. R., and Gargas, M. L. (2010) 1,3-Butadiene: II. Genotoxicity profile. *Crit. Rev. Toxicol. 40* (Suppl 1), 12−73.
(31) United States Environmental Protection Agency (EPA) (2002) *Health Assessment of 1,3-Butadiene*, EPA/600/P-98/001F, National Center for Environmental Assessment, Washington, DC, available from National Technical Information Service, Springfield, VA, http://www.epa.gov/ncea/.
(32) National Toxicology Program (NTP) (2011) 1,3-Butadiene, CAS No. 106-99-0, in *12th Report on Carcinogens (RoC)*, National Toxicology Program, Research Triangle Park, NC. http://ntp.niehs.nih.gov/go/roc12.
(33) International Agency for Research on Cancer (1999) Re-evaluation of some organic chemicals, hydrazine and hydrogen peroxide, IRC Monographs on the Evaluation of Carcinogenic Risks to Humans. *IARC Sci. Publ. 71*, 109−125.
(34) International Agency for Research on Cancer (2008) IARC monographs on the evaluation of carcinogenic risks to humans. Volume 97. 1,3-Butadiene, ethylene oxide and vinyl halides (vinyl fluoride, vinyl chloride and vinyl bromide). *IARC Monogr. Eval. Carcinog. Risks Hum. 97*, 3−471.
(35) Swenberg, J. A., Bordeerat, N. K., Boysen, G., Carro, S., Georgieva, N. I., Nakamura, J., Troutman, J. M., Upton, P. B., Albertini, R. J., Vacek, P. M., Walker, V. E., Sram, R. J., Goggin, M., and Tretyakova, N. (2011) 1,3-Butadiene: Biomarkers and application to risk assessment. *Chem.-Biol. Interact. 192*, 150−154.
(36) Kotapati, S., Sangaraju, D., Esades, A., Hallberg, L., Walker, V. E., Swenberg, J. A., and Tretyakova, N. Y. (2014) Bis-butanediol-mercapturic acid (bis-BDMA) as a urinary biomarker of metabolic activation of butadiene to its ultimate carcinogenic species. *Carcinogenesis*, DOI: 10.1093/carcin/bgu047.
(37) Krause, R. J., Sharer, J. E., and Elfarra, A. A. (1997) Epoxide hydrolase-dependent metabolism of butadiene monoxide to 3- butene-1,2-diol in mouse, rat, and human liver. *Drug Metab. Dispos. 25*, 1013−1015.
(38) Nieusma, J. L., Claffey, D. J., Maniglier-Poulet, C., Imiolczyk, T., Ross, D., and Ruth, J. A. (1997) Stereochemical aspects of 1,3-butadiene metabolism and toxicity in rat and mouse liver microsomes and freshly isolated rat hepatocytes. *Chem. Res. Toxicol. 10*, 450−456.
(39) Nieusma, J. L., Claffey, D. J., Koop, D. R., Chen, W., Peter, R. M., Nelson, S. D., Ruth, J. A., and Ross, D. (1998) Oxidation of 1,3-butadiene to (*R*)- and (*S*)-butadiene monoxide by purified recombinant cytochrome P450 2E1 from rabbit, rat and human. *Toxicol. Lett. 95*, 123−129.

(40) Duescher, R. J., and Elfarra, A. A. (1994) Human liver microsomes are efficient catalysts of 1,3-butadiene oxidation: Evidence for major roles by cytochromes P450 2A6 and 2E1. *Arch. Biochem. Biophys. 311*, 342−349.
(41) Kirman, C. R., Albertini, R. J., Sweeney, L. M., and Gargas, M. L. (2010) 1,3-Butadiene: I. Review of metabolism and the implications to human health risk assessment. *Crit. Rev. Toxicol. 40* (Suppl 1), 1−11.
(42) Kirman, C. R., Albertini, R. A., and Gargas, M. L. (2010) 1,3-Butadiene: III. Assessing carcinogenic modes of action. *Crit. Rev. Toxicol. 40* (Suppl 1), 74−92.
(43) Sasiadek, M., and Chichlowska-Sliwinska, M. (1991) Genotoxic properties of 1,3-butadiene and its derivatives. *Med. Pr. 42*, 193−198.
(44) Cochrane, J. E., and Skopek, T. R. (1994) Mutagenicity of butadiene and its epoxide metabolites: I. Mutagenic potential of 1,2-epoxybutene, 1,2,3,4-diepoxybutane and 3,4-epoxy-1,2-butanediol in cultured human lymphoblasts. *Carcinogenesis 15*, 713−717.
(45) Krause, R. J., and Elfarra, A. A. (1997) Oxidation of butadiene monoxide to meso- and (±)-diepoxybutane by cDNA-expressed human cytochrome P450s and by mouse, rat, and human liver microsomes: Evidence for preferential hydration of meso-diepoxybutane in rat and human liver microsomes. *Arch. Biochem. Biophys. 337*, 176−184.
(46) Verly, W. G., Brakier, L., and Feit, P. W. (1971) Inactivation of the T7 coliphage by the diepoxybutane stereoisomers. *Biochim. Biophys. Acta 228*, 400−406.
(47) Matagne, R. (1969) Induction of chromosomal aberrations and mutations with isomeric forms of L-threitol-I,4-bismethanesulfonate in plant materials. *Mutat. Res. 7*, 241−247.
(48) Kim, M. Y., Tretyakova, N., and Wogan, G. N. (2007) Mutagenesis of the supF gene by stereoisomers of 1,2,3,4-diepoxybutane. *Chem. Res. Toxicol. 20*, 790−797.
(49) Thornton-Manning, J. R., Dahl, A. R., Bechtold, W. E., Griffith, W. C. J., and Henderson, R. F. (1997) Comparison of the disposition of butadiene epoxides in Sprague-Dawley rats and B6c3F1 mice following a single and repeated exposures to 1,3- butadiene via inhalation. *Toxicology 123*, 125−134.
(50) Park, S., Hodge, J., Anderson, C., and Tretyakova, N. (2004) Guanine-adenine DNA cross-Linking by 1,2,3,4-diepoxybutane: Potential basis for biological activity. *Chem. Res. Toxicol. 17*, 1638−1651.
(51) Park, S., and Tretyakova, N. (2004) Structural characterization of the major DNA-DNA cross-link of 1,2,3,4-diepoxybutane. *Chem. Res. Toxicol. 17*, 129−136.
(52) Cochrane, J. E., and Skopek, T. R. (1993) Mutagenicity of 1,3-Butadiene and Its Epoxide Metabolites in Human TK6 Cells and in Splenic T Cells Isolated from Exposed C6c3F1 Mice, in *Butadiene and Styrene, Assessment of Health Hazards*, IARC Scientific Publications Series, Vol. *127*, pp 195−204, IARC, Lyon, France.
(53) Cochrane, J. E., and Skopek, T. R. (1994) Mutagenicity of butadiene and its epoxide metabolites: II. Mutational spectra of butadiene, 1,2-epoxybutene and diepoxybutane at the hprt locus in splenic T cells from exposed B6c3F1 mice. *Carcinogenesis 15*, 719−723.
(54) Seneviratne, U., Antsypovich, S., Goggin, M., Dorr, D. Q., Guza, R., Moser, A., Thompson, C., York, D. M., and Tretyakova, N. (2010) Exocyclic deoxyadenosine adducts of 1,2,3,4-diepoxybutane: Synthesis, structural elucidation, and mechanistic studies. *Chem. Res. Toxicol. 23*, 118−133.
(55) Feng, B., and Stone, M. P. (1995) Solution structure of an oligodeoxynucleotide containing the human N- ras codon 61 sequence refined from ^{1}H NMR using molecular dynamics restrained by nuclear Overhauser effects. *Chem. Res. Toxicol. 8*, 821−832.
(56) Seneviratne, U., Antsypovich, S., Dorr, D. Q., Dissanayake, T., Kotapati, S., and Tretyakova, N. (2010) DNA oligomers containing site-specific and stereospecific exocyclic deoxyadenosine adducts of 1,2,3,4-diepoxybutane: Synthesis, characterization, and effects on DNA structure. *Chem. Res. Toxicol. 23*, 1556−1567.
(57) Nechev, L. V., Zhang, M., Tsarouhtsis, D., Tamura, P. J., Wilkinson, A. S., Harris, C. M., and Harris, T. M. (2001) Synthesis and characterization of nucleosides and oligonucleotides bearing adducts of butadiene epoxides on adenine N^6 and guanine N^2. *Chem. Res. Toxicol. 14*, 379−388.
(58) Kim, S. J., Stone, M. P., Harris, C. M., and Harris, T. M. (1992) A postoligomerization synthesis of oligodeoxynucleotides containing polycyclic aromatic hydrocarbon adducts at the N^6 position of deoxyadenosine. *J. Am. Chem. Soc. 114*, 5480−5481.
(59) Kim, H.-Y., Nechev, L., Zhou, L., Tamura, P., Harris, C. M., and Harris, T. M. (1998) Synthesis and adduction of fully deprotected oligodeoxynucleotides containing 6-chloropurine. *Tetrahedron Lett. 39*, 6803−6806.
(60) Cavaluzzi, M. J., and Borer, P. N. (2004) Revised UV extinction coefficients for nucleoside-5′-monophosphates and unpaired DNA and RNA. *Nucleic Acids Res. 32*, e13.
(61) Jeener, J., Meier, B. H., Bachmann, P., and Ernst, R. R. (1979) Investigation of exchange processes by 2-dimensional NMR spectroscopy. *J. Chem. Phys. 71*, 4546−4553.
(62) Wagner, R., and Berger, S. (1996) Gradient-selected NOESY - A fourfold reduction of the measurement time for the NOESY experiment. *J. Magn. Res. A 123*, 119−121.
(63) Piantini, U., Sorensen, O. W., and Ernst, R. R. (1982) Multiple quantum filters for elucidating NMR coupling networks. *J. Am. Chem. Soc. 104*, 6800−6801.
(64) Piotto, M., Saudek, V., and Sklenar, V. (1992) Gradient-tailored excitation for single-quantum NMR spectroscopy of aqueous solutions. *J. Biomol. NMR 6*, 661−665.
(65) Goddard, T. D., and Kneller, D. G. (2006) *SPARKY*, v. 3.113. University of California, San Francisco, CA.
(66) James, T. L. (1991) Relaxation matrix analysis of two-dimensional nuclear Overhauser effect spectra. *Curr. Opin. Struct. Biol. 1*, 1042−1053.
(67) Keepers, J. W., and James, T. L. (1984) A theoretical study of distance determination from NMR. Two-dimensional nuclear Overhauser effect spectra. *J. Magn. Reson. 57*, 404−426.
(68) Borgias, B. A., and James, T. L. (1990) MARDIGRAS–a procedure for matrix analysis of relaxation for discerning geometry of an aqueous structure. *J. Magn. Reson. 87*, 475−487.
(69) Tonelli, M., and James, T. L. (1998) Insights into the dynamic nature of DNA duplex structure via analysis of nuclear Overhauser effect intensities. *Biochemistry 37*, 11478−11487.
(70) Arnott, S., and Hukins, D. W. L. (1972) Optimised parameters for A-DNA and B-DNA. *Biochem. Biophys. Res. Commun. 47*, 1504−1509.
(71) Case, D. A., Cheatham, T. E., III, Darden, T., Gohlke, H., Luo, R., Merz, K. M., Jr., Onufriev, A., Simmerling, C., Wang, B., and Woods, R. J. (2005) The AMBER biomolecular simulation programs. *J. Comput. Chem. 26*, 1668−1688.
(72) Wang, J. M., Cieplak, P., and Kollman, P. A. (2000) How well does a restrained electrostatic potential (RESP) model perform in calculating conformational energies of organic and biological molecules? *J. Comput. Chem. 21*, 1049−1074.
(73) Frisch, M. J., Trucks, G. W., Schlegel, H. B., Scuseria, G. E., Robb, M. A., Cheeseman, J. R., Montgomery, J. A., Vreven, T., Kudin, K. N., Burant, J. C., Millam, J. M., Iyengar, S. S., Tomasi, J., Barone, V., Mennucci, B., Cossi, M., Scalmani, G., Rega, N., Petersson, G. A., Nakatsuji, H., Hada, M., Ehara, M., Toyota, K., Fukuda, R., Hasegawa, J., Ishida, M., Nakajima, T., Honda, Y., Kitao, O., Nakai, H., Klene, M., Li, X., Knox, J. E., Hratchian, H. P., Cross, J. B., Adamo, C., Jaramillo, J., Gomperts, R., Stratmann, R. E., Yazyev, O., Austin, A. J., Cammi, R., Pomelli, C., Pomelli, J., Ochterski, W., Ayala, P. Y., Morokuma, K., Voth, G. A., Salvador, P., Dannenberg, J. J., Zakrzewska, V. G., Daniels, A. D., Farkas, O., Rabuck, A. D., Raghavachari, K., and Ortiz, J. V. (2004) *GAUSSIAN 03*, Gaussian, Inc., Wallingford, CT.
(74) Schafmeister, C. E. A., Ross, W. S., and Romanovski, V. (1995) *XLEAP*, University of California, San Francisco, CA.
(75) Kirkpatrick, S., Gelatt, C. D., Jr., and Vecchi, M. P. (1983) Optimization by simulated annealing. *Science 220*, 671−680.

(76) Bashford, D., and Case, D. A. (2000) Generalized Born models of macromolecular solvation effects. *Annu. Rev. Phys. Chem. 51*, 129−152.
(77) Berendsen, H. J. C., Postma, J. P. M., van Gunsteren, W. F., DiNola, A., and Haak, J. R. (1984) Molecular dynamics with coupling to an external bath. *J. Phys. Chem. 81*, 3684−3690.
(78) Blanchet, C., Pasi, M., Zakrzewska, K., and Lavery, R. (2011) CURVES+ web server for analyzing and visualizing the helical, backbone and groove parameters of nucleic acid structures. *Nucleic Acids Res. 39*, W68−73.
(79) Patel, D. J., Shapiro, L., and Hare, D. (1987) DNA and RNA: NMR studies of conformations and dynamics in solution. *Q. Rev. Biophys. 20*, 35−112.
(80) Reid, B. R. (1987) Sequence-specific assignments and their use in NMR studies of DNA structure. *Q. Rev. Biophys. 20*, 2−28.
(81) Boelens, R., Scheek, R. M., Dijkstra, K., and Kaptein, R. (1985) Sequential assignment of imino- and amino-proton resonances in ^{1}H NMR spectra of oligonucleotides by two-dimensional NMR spectroscopy. Application to a *lac* operator fragment. *J. Magn. Reson. 62*, 378−386.
(82) Xu, W., Merritt, W. K., Nechev, L. V., Harris, T. M., Harris, C. M., Lloyd, R. S., and Stone, M. P. (2007) Structure of the 1,4-bis(2′-deoxyadenosin-N^6-yl)-2*S*,3*S*-butanediol intrastrand DNA cross-link arising from butadiene diepoxide in the human *N-ras* codon 61 sequence. *Chem. Res. Toxicol. 20*, 187−198.
(83) Lawley, P. D., and Brookes, P. (1967) Interstrand cross-linking of DNA by difunctional alkylating agents. *J. Mol. Biol. 25*, 143−160.
(84) Recio, L., Steen, A. M., Pluta, L. J., Meyer, K. G., and Saranko, C. J. (2001) Mutational spectrum of 1,3-butadiene and metabolites 1,2-epoxybutene and 1,2,3,4-diepoxybutane to assess mutagenic mechanisms. *Chem.-Biol. Interact. 135*−*136*, 325−341.
(85) Steen, A. M., Meyer, K. G., and Recio, L. (1997) Analysis of hprt mutations occurring in human TK6 lymphoblastoid cells following exposure to 1,2,3,4-diepoxybutane. *Mutagenesis 12*, 61−67.
(86) Carmical, J. R., Nechev, L. V., Harris, C. M., Harris, T. M., and Lloyd, R. S. (2000) Mutagenic potential of adenine N^6 adducts of butadience mono- and diepoxide. *Mutagenesis 35*, 48−56.
(87) Scholdberg, T. A., Nechev, L. V., Merritt, W. K., Harris, T. M., Harris, C. M., Lloyd, R. S., and Stone, M. P. (2005) Mispairing of a site specific major groove (2*S*,3*S*)-N^6-(2,3,4-trihydroxybutyl)-2′-deoxyadenosyl DNA adduct of butadiene diol epoxide with deoxyguanosine: Formation of a dA(*anti*):dG(*anti*) pairing interaction. *Chem. Res. Toxicol. 18*, 145−153.
(88) Feng, B., Zhou, L., Passarelli, M., Harris, C. M., Harris, T. M., and Stone, M. P. (1995) Major groove (*R*)-alpha-(N^6-adenyl)styrene oxide adducts in an oligodeoxynucleotide containing the human *N-ras* codon 61 sequence: Conformations of the *R*(61,2) and *R*(61,3) sequence isomers from ^{1}H NMR. *Biochemistry 34*, 14021−14036.
(89) Stone, M. P., and Feng, B. (1996) Sequence and stereospecific consequences of major groove (N^6-adenyl)-styrene oxide adducts in an oligodeoxynucleotide containing the human *N-ras* codon 61 sequence. *Magn. Reson. Chem. 34*, S105−S114.
(90) Feng, B., Voehler, M. W., Zhou, L., Passarelli, M., Harris, C. M., Harris, T. M., and Stone, M. P. (1996) Major groove *S*-alpha-(N^6-adenyl)-styrene oxide adducts in an oligodeoxynucleotide containing the human *N-ras* codon 61 sequence: Conformations of the *S*(61,2) and *S*(61,3) sequence isomers from ^{1}H NMR. *Biochemistry 35*, 7316−7329.
(91) Hennard, C., Finneman, J., Harris, C. M., Harris, T. M., and Stone, M. P. (2001) The nonmutagenic (*R*)- and (*S*)-beta-(N^6-adenyl)styrene oxide adducts are oriented in the major groove and show little perturbation to DNA structure. *Biochemistry 40*, 9780−9791.
(92) Merritt, W. K., Scholdberg, T. A., Nechev, L. V., Harris, T. M., Harris, C. M., Lloyd, R. S., and Stone, M. P. (2004) Stereospecific structural perturbations arising from adenine N^6 butadiene triol adducts in duplex DNA. *Chem. Res. Toxicol. 17*, 1007−1019.
(93) Scholdberg, T. A., Nechev, L. V., Merritt, W. K., Harris, T. M., Harris, C. M., Lloyd, R. S., and Stone, M. P. (2004) Structure of a site specific major groove (2*S*,3*S*)-N^6-(2,3,4-trihydroxybutyl)-2′-deoxyadenosyl DNA adduct of butadiene diol epoxide. *Chem. Res. Toxicol. 17*, 717−730.
(94) Wickramaratne, S., Goggin, M., Li, D., Delaney, J., He, C., Essigmann, J., and Tretyakova, N. (2013) *In vitro* Repair Studies of 1,3-Butadiene Induced Adenine Lesions, [Abstract], Division of Chemical Toxicology, 246th ACS National Meeting, Sep 8−12, 2013, Indianapolis, IN.
(95) Essigmann, J. M. Massachusetts Institute of Technology, Cambridge, Massachusetts. Personal communication, 2012.
(96) Kotapati, S., Maddukuri, L., Wickramaratne, S., Seneviratne, U., Pence, M., Marnett, L., and Tretyakova, N. (2012) Translesion Synthesis across 1,3-Butadiene-Induced Deoxyadenosine Adducts, [Abstract], Division of Chemical Toxicology, 244th National Meeting of the American Chemical Society (ACS), Aug 19−23, 2012, Philadelphia, PA.
(97) Kowal, E. A., Seneviratne, U., Wickramaratne, S., Tretyakova, N., and Stone, M. P. (2011) Structural Investigation of Exocyclic Deoxyadenosine Adducts Induced by 1,2,3,4-Diepoxybutane [Abstract], Division of Chemical Toxicology, 242nd National Meeting of the American Chemical Society (ACS), Aug 28-Sep 01, 2011, Denver, CO.